Origins of Folding Instabilities on Polycrystalline Metal Surfaces

N. Beckmann,[1,2] P. A. Romero,[1] D. Linsler,[1,2] M. Dienwiebel,[1,2] U. Stolz,[3] M. Moseler,[1,4,*] and P. Gumbsch[1,2]

[1]*Fraunhofer Institute for Mechanics of Materials IWM, MicroTribology Center TC, Wöhlerstrasse 11, 79108 Freiburg, Germany*

[2]*Karlsruhe Institute of Technology, Institute for Applied Materials IAM, Kaiserstrasse 12, 76131 Karlsruhe, Germany*

[3]*Robert Bosch GmbH, Robert-Bosch-Platz 1, 70839 Gerlingen-Schillerhöhe, Germany*

[4]*Faculty of Physics, University of Freiburg, Hermann-Herder-Strasse 3, 79104 Freiburg, Germany*

(Received 24 April 2014; revised manuscript received 18 November 2014; published 4 December 2014)

Wear and removal of material from polycrystalline metal surfaces is inherently connected to plastic flow. Here, plowing-induced unconstrained surface plastic flow on a nanocrystalline copper surface has been studied by massive molecular dynamics simulations and atomic force microscopy scratch experiments. In agreement with experimental findings, bulges in front of a model asperity develop into vortexlike fold patterns that mark the disruption of laminar flow. We identify dislocation-mediated plastic flow in grains with suitably oriented slip systems as the basic mechanism of bulging and fold formation. The observed folding can be fundamentally explained by the inhomogeneity of plasticity on polycrystalline surfaces which favors bulge formation on grains with suitably oriented slip system. This process is clearly distinct from Kelvin-Helmholtz instabilities in fluids, which have been previously suggested to resemble the formed surface fold patterns. The generated prow grows into a rough chip with stratified lamellae that are identified as the precursors of wear debris. Our findings demonstrate the importance of surface texture and grain structure engineering to achieve ultralow wear in metals.

DOI: 10.1103/PhysRevApplied.2.064004

I. INTRODUCTION

Understanding the unconstrained plastic flow (UPF) of polycrystalline metallic surfaces in sliding contact with hard asperities is crucial for the control of wear in metal-based tribological systems [1–3] and the generation of surfaces in metal-working processes [4–7]. The wear resistance of metallic machine parts can be influenced by preconditioning—either by the final manufacturing steps [8,9] (such as lapping, honing, and grinding) or by suitable running-in procedures during the initial life of a tribological contact [10]. Both modify the topography, as well as the crystalline structure and chemical composition in the near-surface material [8]. The intricate interplay between these three structural properties complicates the determination of optimum initial conditions and consequently tedious trial-and-error experiments have to be performed to improve wear resistance in metallic materials. Of course, a mechanism based understanding of UPF would guide practitioners towards an intelligent design of wear-resistant metal surfaces thus drastically reducing the number of trial-and-error cycles.

Traditionally, models of UPF have been based on smooth laminar material displacement [3]—an assumption whose general validity has been recently challenged by *in situ* observations of the disruption of laminar flow via folding on a microcrystalline copper surface sliding against a hard steel wedge [11]. The resemblance of the observed vortexlike fold structures to patterns arising from Kelvin-Helmholtz-type instabilities in fluids [12] led to the interpretation of folding as a fluidlike flow instability indicative of a confined early stage of turbulence [11]. Atomistic simulations reporting Kelvin-Helmholtz patterns in plastic flow between sliding monocrystalline surfaces [13] were quoted to support this conjecture [11]. Bulges that arose at a distance of a couple of grain diameters in front of the wedge were subsequently compared with undulating protuberances of fluids near hydraulic jumps [14].

Interestingly, the authors of Ref. [11] only observed folds in their accompanying finite-element (FE) simulations with a two-phase model (composed of soft and hard grains) suggesting that crystal plasticity causes folding and not a fluidlike instability. Unfortunately, FE lacks the description of the atomistic and crystallographic details underlying the deformation mechanisms responsible for the folding process. Consequently, the microscopic origins of UPF-induced folds in polycrystalline metallic surfaces remain elusive (despite the impressive progress of *in situ* [11,15–17] and *ex situ* [18,19] microscopy techniques for the observation of tribological systems).

In this article, we use large-scale atomistic simulations to shed light on the basic mechanisms underlying fold formation during UPF. We demonstrate in detail that bulges in front of a moving indenter with a −45° rake angle are

*michael.moseler@iwm.fraunhofer.de

localized on grains with slip systems that are favorably oriented with respect to the indenter's cutting plane while the surface of unsuitably oriented grains remains smooth. This implies that even though the subsequently formed surface folds might resemble the early stages of a vortex, they are a consequence of the orientation anisotropy on the granular length scale and not of a fluidlike flow instability. Our simulations are supported by an atomic force microscope (AFM) scratch experiment that reveals strikingly similar fold patterns. These results suggest a notable improvement of wear resistance by a preconditioning that produces a suitable anisotropic crystallographic texture in the near-surface region of metals.

II. METHODS

A. Simulation approach

The plowing of a nanocrystalline (nc) copper surface by a rigid tapered indenter is studied by massive parallel molecular dynamics (MD) [20] employing an embedded-atom method potential [21]. The surface is modeled as a $160 \times 40 \times 30$ nm^3 block [see Fig. 1(a)]. To construct the copper surface, a Voronoi algorithm is used to create a fully periodic system with 1584 randomly oriented grains with grain diameters ranging from 4 to 12 nm. The constructed substrate contains 15 409 694 atoms after removing atoms closer than 0.16 nm within the grain boundaries. The initial Voronoi construction is first optimized with the fast inertial relaxation engine (FIRE) [22] before annealing the sample by heating and holding it at 80% of the melting temperature ($T_m = 1152$ K) for 500 ps followed by cooling it to 300 K within 50 ps and finally holding the sample at 300 K for 50 ps in order to create a system with relaxed grains and grain boundaries. The temperature changes are conducted within 10 ps respectively with a Berendsen thermostat [23] while holding the pressure constant at 0 GPa with a Berendsen barostat.

During annealing, the system dimensions shrink to $158.8 \times 39.5 \times 29.6$ nm^3. After annealing, the system acquired an approximate log normal distribution of grains ranging in size from 4 to 18 nm. Despite being limited to nanosized grains, the modeled distribution of grain sizes and grain orientations is common in conventional polycrystalline metals, which typically exhibit a log normal distribution of grain sizes and a random distribution of grain orientations.

The last 40 ps of annealing were performed without periodic boundary conditions in the z direction to achieve surface relaxation. This yields a negligible surface height difference of less than 1 nm.

Also during the plowing simulations, periodic boundary conditions are employed in the lateral directions and a 0.5 nm layer of fixed atoms at the bottom of the block mimics the anchoring of the resulting Cu nanofilm to a large sample. The indenter is modeled as a nonreactive rigid wedge [with a 90° opening angle; see Fig. 1(a)] interacting with the Cu surface via a harmonically repulsive potential with a stiffness of 32 N m^{-1} per atom and a 0.5 nm cutoff. A 300 K thermostat is applied to all atoms in the system in order to reflect ambient temperature and to reduce

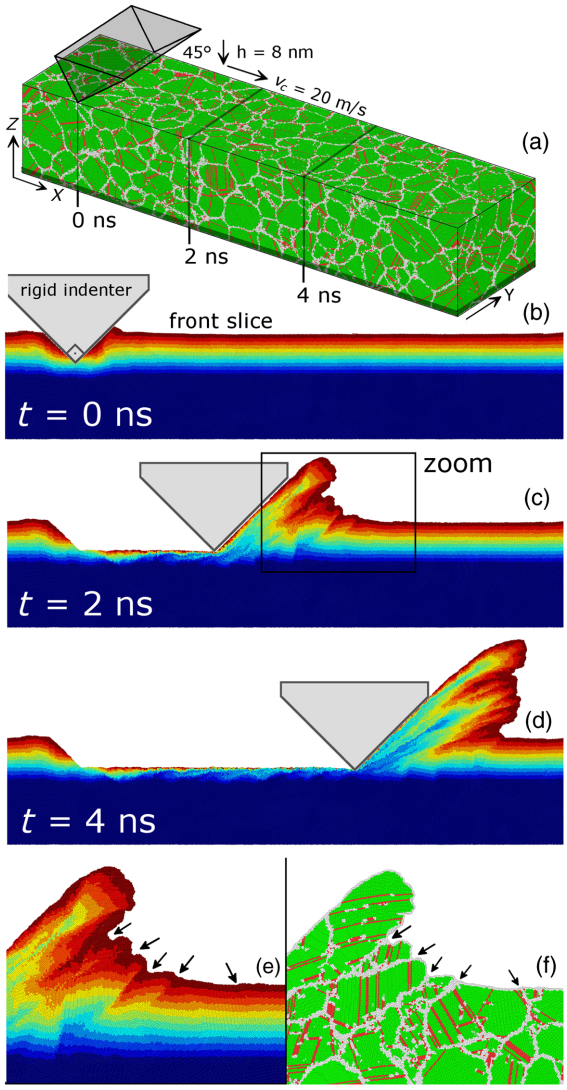

FIG. 1. Molecular dynamics simulation of unconstrained surface plastic flow. (a) Copper nanocrystalline substrate and rigid indenter model. Atoms are colored according to their local environment using a common neighbor analysis (CNA) [24]. Green spheres represent atoms with an fcc environment; red spheres indicate stacking fault and twin boundary atoms; and gray spheres locate GBs and other defect sites. The grains are randomly oriented and contain defects characteristic of annealed copper [25–28]. (b)–(d) Sequence of snapshots [at the times and indenter positions indicated in Fig. 1(a)] showing an xz cross section of the Cu block. The atoms have been colored according to their initial vertical position revealing the initiation and evolution of folding patterns during plowing. (e) Close-up of the chip shown in Fig. 1(c). (f) Same as (e) but colored according to CNA.

thermally induced grain growth [25,29] in nc-Cu. Note that in metallic solids, heat conduction predominantly occurs through electronic excitation. Therefore, conventional classical molecular dynamics (where only ionic degrees of freedom are modeled) cannot adequately capture heat generation and propagation in metals such as copper. One approach to conduct thermally accurate MD simulations for metals is to thermalize the whole system to the desired temperature. Along these lines, the entire nanocrystalline system presented here is thermalized during indentation and plowing using a dissipative particle dynamics (DPD) thermostat [30] with a dissipation constant of 0.1 eV ps Å^{-2} and a cutoff of 0.45 nm. DPD thermostats are Galilean invariant and therefore do not bias the velocity profile and do not add an artificial drag to the observed deformation.

B. Experimental approach

Nanoindentation and plowing experiments are performed on a nanocrystalline Cu substrate using an atomic force microscope tip. To generate the nanocrystalline Cu surface, a pure (99.98 wt %) oxygen-free highly conductive (OFHC) microcrystalline Cu sample is first polished with a 1 μm diamond particle suspension and subsequently scratched with a reciprocating natural diamond AFM tip (Bruker PDNISP) at a normal force of 134 μN. Focused ion beam (FIB) cross sections reveal the formation of a nanocrystalline Cu surface layer [31] with approximately 100-nm-sized grains. The plowing tests are performed with a PDNISP probe (Bruker, formerly Veeco) designed for nanoindentation experiments. The indentation probe consists of a diamond tip mounted on a stainless steel cantilever with a calibrated spring constant of 211 N m^{-1}. The diamond tip apex is the corner of a cube formed by three right angles (see the Supplemental Material [32], Fig. S5). The vertical axis of the pyramid is approximately normal to the sample when mounted on the atomic force microscope. The AFM used is a Dimension V (Bruker, formerly Veeco) with a Nanoscope V controller (Digital Instruments). The tip is moved at 0.1 Hz over a scan size of 20×20 μm^2 yielding a horizontal scan speed of 4 μm s^{-1}. The applied normal load is approximately 134 μN. A complete trace of the wear track generated by the nanoindentation tip can be seen in the Supplemental Material [32], Fig. S6 where black lines mark the trajectory. Cross sections of the wear track were extracted with a Helios NanoLab 650 DualBeam microscope (FEI). Platinum-rich protective layers were deposited prior to preparing cross sections using an electron- and ion-beam-induced deposition. The secondary-electron picture of the cross section through the chip was scanned with a current of 50 pA and 2 kV at a tilt angle of 52°. No FIB secondary-electron images were postprocessed for tilt correction.

III. RESULTS AND DISCUSSION

Prior to plowing, the surface is indented to a depth of $h = 8$ nm with a velocity of $v_i = 20$ m s^{-1} resulting in significant material pileup; see cross-sectional view in Fig. 1(b) colored according to the initial vertical position of the atoms (abbreviated throughout this paper as initial-z color scheme). Subsequently, the nc copper is plowed at constant h and a velocity of $v_c = 20$ m s^{-1}.

The buildup of pronounced fold patterns can be observed during the simulations. Figure 1(c) shows a snapshot of the system at $t = 2$ ns (see the Supplemental Material [32] for a movie of the plowing). The folding leads to the formation of a chip with a rough front face [Fig. 1(d)]. Similarities to the micron-scale folds of Ref. [11] are apparent. Note that folding is not restricted to Cu since it can also be observed in simulations for other fcc metals (see the Supplemental Material [32] for simulations with Pt [33], Ni [34], and Ag [35] potentials).

By inspecting the microstructure of the copper film, the mechanisms that govern the induced surface folding can be detected. A close-up of the chip in Fig. 1(c) (marked by a black frame) is shown in Fig. 1(e) along with additional arrows that mark the notches between the surface protrusions. The observed notches occur consistently at grain boundaries (GB): Fig. 1(f) shows a common neighbor analysis [24] for the atoms in Fig. 1(e). Clearly, the arrows coincide with gray zones in Fig. 1(f) representing GBs that separate crystalline areas (green zones).

At some arrows in Fig. 1(e), discontinuities in the strata of the initial-z color scheme can be discerned at GBs which may indicate GB sliding [36] as one mechanism that plays a role in the initiation of bulging and fold formation in nc metals. However, in general bulging of surface grains during UPF occurs mainly through dislocation-mediated plasticity (for a further discussion, see the Supplemental Material [32]). This finding is somewhat surprising, since uniaxial deformation experiments of nanocrystalline copper at grain sizes below ≈20 nm show very limited plastic deformation before fracture [37,38] and also corresponding simulations mostly show other relaxation processes in the grain boundaries instead of dislocation-mediated plasticity [36,39,40]. The behavior can however be rationalized if one considers that the action of the indenter on the surface locally necessitates a specific mode of deformation and can lead to extremely high local stresses. Indeed, the mean shear stresses in front of the indenter can reach values on the order of 5 GPa and stress peaks at grain boundaries may be significantly higher so that dislocations can be easily nucleated at grain boundaries between grains in front of the indenter.

In the following, the bulging is analyzed in more detail. The geometric form of the indenter with a −45° rake angle suggests that an optimal crystal orientation for outward flow contains a slip system whose slip direction coincides with the rake face and motion of the indenter. This idea is

supported by the literature on metal machining that reports shear zones parallel to the cutting edge [41].

In order to quantify the ability of an atomic environment to support a certain shear deformation, an atomic stress projection factor (ASPF) is defined as follows. First, for each atom with an fcc environment, the projections $m_s = \cos\varphi_s \cos\lambda_s$ are calculated for the $s = 1, \ldots, 12$ fcc slip systems. Here, λ_s are the angles between the normal of the indenter's rake face and the normals of the $\{111\}$ slip planes of the atomic fcc environment. φ_s denote the angles between chip flow direction (reflecting the upward material transport along the $-45°$ rake angle) and the $\langle 110 \rangle$ slip directions of the atomic fcc environment of the grain. The ASPF is defined as the maximum m_s of the 12 fcc slip systems similar to the Schmid factor for uniaxial deformation.

The evolution of the ASPF is shown in Fig. 2 for a xz cross-sectional slice of the Cu sample. Regions with different ASPF are separated by grain and twin boundaries (depicted in Fig. 2 as gray and pink lines, respectively). During indentation ($t < 0$ ns), the large twinned grain G_1 with low ASPF (≈0.7) has been pushed to the right, exerting compressive stress on grain G_2. The ASPF of G_2 (≈0.9) is higher, indicating that one of its slip systems supports shear deformation parallel to the rake face of the indenter. This has produced a first little bulge on the surface of G_2 during indentation [see Fig. 2(a) at $t = 0$ ns]. Such a bulge does not always develop. It is for instance missing on the left-hand side of the indenter in Fig. 1(b) due to a grain with low ASPF (≈0.6).

By subsequent plowing, grains G_1 and G_2 are pushed further by the indenter. The ASPF in G_2 is still higher than G_1 and therefore both grains continue to deform differently [see Fig. 2(b)]. In contrast to G_1, which continues to resist bulging, the bulge on G_2 has moved significantly upward, as it realigns (during its plastic deformation) into an orientation with even higher ASPF (≈1.0). Concurrently, G_3 has also started to deform, accompanied by the consumption of grains in its neighborhood such as the upper part of G_4 [Fig. 2(b)]. The growth of G_3 by migration of its grain boundaries continues creating an extended vertically elongated region $G_2 + G_3$ [see large red region in Fig. 2(c) at $t = 0.4$ ns] with ideally aligned slip systems and a large bulge.

In the meantime, the neighboring grains started to change their structure. Grain G_5 as well as its right-hand side neighbor G_6 are twinned [Fig. 2(b) shows the undeformed structures]. Interestingly, G_5 and G_6, which consist of twin regions with low ASPF (≈0.6) and high ASPF (≈0.8 to 0.9) [see Fig. 2(c)], only undergo slight bulging and are later overflown by the coarsened $G_2 + G_3$ grain [see Fig. 2(d)], which has a high ASPF (≈1.0). During further plowing, the deformation of G_6 continues [see Fig. 2(d)] accompanied by lattice reorientation that lowers the ASPF (≈0.7) and stops the bulging process. Further GB migration and even the nucleation of new grains dominate the processes in the chip.

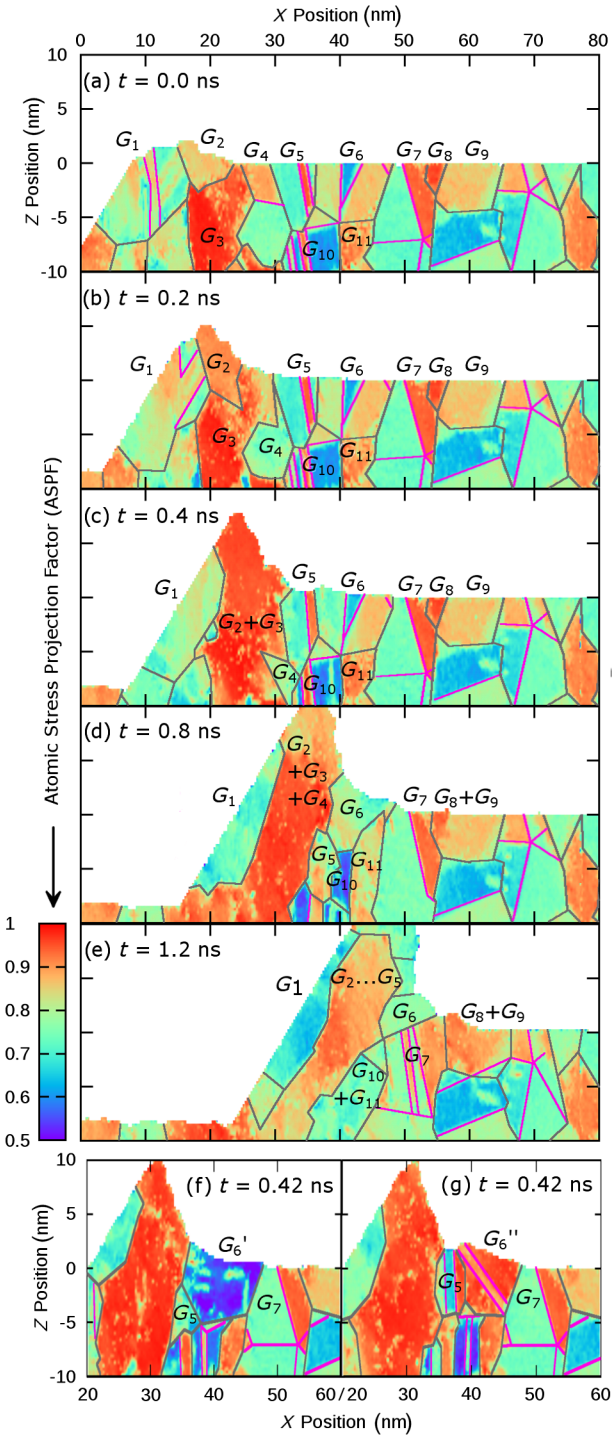

FIG. 2. Temporal evolution of atomic stress projection factor. In addition to the color coding according to the ASPF, GBs are marked in gray and twins in pink.

Grain G_7 is similar to G_5, having a large twin region with low ASPF (≈0.7) and a smaller one with high ASPF (≈0.9). Consequently, the plastic upward flow of G_7 is hindered, while GB migration allows parts of the favorably oriented twin of G_7 and the next grains G_8 and G_9 to merge. All these regions have high ASPF

(≈1.0) and are forming again a pronounced bulge [see Fig. 2(e)].

From this detailed history of deformation events, a new mechanism for fold formation can be deduced. Bulge formation on the surface of grains with high ASPF constitutes the necessary first step of folding. Note that low ASPF grains also deform, but without bulging. In order to provide further evidence for this, two additional simulations are carried out [see Figs. 2(f) and 2(g)]. Grain G_6 in Fig. 2(c) is either replaced by a grain with low ASPF (G_6' with 0.5) or by a grain with high ASPF (G_6'' with 1.0). Indeed, the surface of the former stays smooth [Fig. 2(f)] while the latter develops a bulge [Fig. 2(g)] as well as a kink at the GB between grains G_5 and G_6''.

From the evolution of the grain structure in Fig. 2, a second mechanism that acts during the plowing of nc materials becomes evident. Right from the start of the plowing, grains in the chip merge and form a large super grain [see for instance $G_2 \cdots G_5$ in Fig. 2(e)]. The underlying mechanisms are lattice reorientation, by which G_2 and G_3 merge, and grain boundary migration, by which $G_2 + G_3$ consumes G_4 in Figs. 2(b)–(d). Both mechanisms lead to a coarsening of the microstructure. At $t = 6.5$ ns, almost the entire chip consists of a single large grain spanning both lateral directions [see Fig. 3(a) and the Supplemental Material [32]].

Both processes—bulging and coarsening—are evidently linked with the motion of dislocations and their interaction with the GBs. While dislocation-assisted GB migration may generally occur in deforming materials [42] and contribute to the deformation of polycrystalline materials by shear coupling [43], it can also contribute by clearing the path for plastic slip towards the surface in favorably oriented grains and by straightening the GBs parallel to suitably oriented slip planes.

Since our simulations have been performed for pure Cu without reactive surface layers (such as oxides or carbon overlayers), one might ask if folding also appears on nc copper under ambient conditions. Therefore, we have conducted a plowing experiment of nc-Cu in ambient air. The nanoindentation tip has the shape of a cube corner (i.e., the apex is formed by three orthogonal faces) resulting in an asymmetric wear scar [Fig. 3(d)]. In our experiment, plowing to the left was performed with an edge, while plowing to the right was performed with a face of the cube. Note that the latter resembles the plowing in our simulations.

After two reciprocating cycles, the tip is stopped in the wear track during rightward plowing and removed in the perpendicular direction leaving behind a small chip [located under the blue rectangle indicating the location of the FIB cut in Fig. 3(d)]. A side view of the chip exhibits striking similarity with our simulated folding pattern. The dark cracklike regions between the elongated grains suggest that passivating layers (e.g., oxides) from the initial surface have been incorporated inside the chip in agreement with the arrest of external surfaces inside the simulated chip. As shown in the Supplemental Material [32], further reciprocating sliding leads to splitting of chips [such as the one in Fig. 3(c)] into nanolamellae, which are the precursors of lamellar wear debris often observed in experiments.

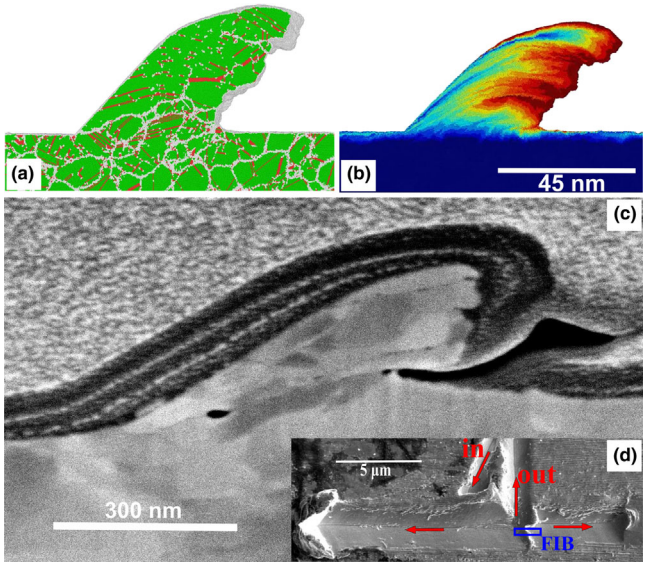

FIG. 3. Comparison of the final chip in the plowing simulation (at $t = 6.5$ ns) with a chip formed by experimentally plowing a nc copper surface with an atomic force microscopy tip. Shown are chip cross sections from the atomistic simulation with (a) CNA color code and (b) initial-z color code. (c) A FIB cross-sectional side view of the experimental chip. (d) Inset displaying a top view of the wear track with the motion of the tip marked by red arrows and the location of the FIB cut over the chip marked by a blue rectangle.

IV. SUMMARY AND CONCLUSIONS

In conclusion, our large-scale MD simulations show that differently oriented slip systems between neighboring surface grains allow soft grains to form protrusions and bulges between hard grains. Projecting the slip systems onto the geometry of the indenter motion allows us to differentiate between soft and hard grain orientations. Grain boundary migration can orient GBs parallel to active slip systems in soft grains. As indicated in Figs. 1(e) and 1(f), GB sliding and GB migration do not contribute significantly to the overall plastic slip because GBs often mark the intrusions between folds in Figs. 1.

Our simulation conditions (thermostat and sliding velocity) mitigate processes (such as grain boundary diffusion, grain-boundary-sliding-mediated rotations, and creep) that are responsible for the plasticity in nanocrystalline metals at higher temperatures or lower speeds [39]. Instead, the chosen conditions favor dislocation-mediated processes that are by no means restricted to nanoscale grains but are rather well documented for texture formation in

conventional polycrystalline metals [44] (see the Supplemental Material [32]). Therefore, plasticity-induced bulging around surface extending lattice defects (e.g., GBs) can be regarded as the elementary process underlying fold formation in polycrystalline metals, which represents an important mechanism for the generation of lamellar wear debris (as suggested by our nanowear experiments). Interestingly, a plastic inhomogeneity was also empirically introduced in the FE simulations of Ref. [11] by employing hard and soft grains, but without referring to slip systems and in disagreement with speculations about fluidlike flow instabilities. Our simulations show unambiguously that visual similarities between the generated folds and Kelvin-Helmholtz vortices in fluids are accidental and folding is clearly governed by the plasticity inhomogeneity of polycrystalline surfaces.

Moreover, our findings suggest a novel engineering approach. Preconditioning of polycrystalline surfaces with grain orientation textures [45–47] via severe plastic deformation [48,49] or machining methods [50] combined with grain boundary doping [51,52] to prevent grain growth could be used to significantly reduce fold formation which in turn would translate into an increase in wear resistance. Keeping the phenomenological nature of current wear prediction models in mind, there is an urgent need for basic atomic level understanding such as the one reported here to guide the design of wear-resistant metallic surfaces. Our results should stimulate further experimental and theoretical work on textured [45–47] and nanocrystalline [25,39,53] surfaces in order to establish guidelines to engineer low-wear metallic surfaces.

ACKNOWLEDGMENTS

Financial support from the Deutsche Forschungsgemeinschaft and the Robert Bosch GmbH is gratefully acknowledged. We thank T. T. Järvi and L. Pastewka for technical help and fruitful discussions. The authors gratefully acknowledge the computing time granted by the John von Neumann Institute for Computing (NIC) provided on the supercomputers JUROPA and JUQUEEN at the Jülich Supercomputing Centre (JSC). Visualization was partially carried out with OVITO [54,55].

N. B. and P. A. R. carried out the simulations and contributed equally to this work.

[1] Frank Philip Bowden and David Tabor, *The Friction and Lubrication of Solids* (Clarendon Press, Oxford, 1950).
[2] F. P. Bowden, A. J. W. Moore, and D. Tabor, The ploughing and adhesion of sliding metals, J. Appl. Phys. **14**, 80 (1943).
[3] K. L. Johnson, Contact mechanics and the wear of metals, Wear **190**, 162 (1995).
[4] P. L. B. Oxley, *The Mechanics of Machining: An Analytical Approach to Assessing Machinability* (Halsted Press, New York, 1989).
[5] Viktor P. Astakhov, *Tribology of Metal Cutting* (Elsevier, New York, 2006), Vol. 52.
[6] P. A. Romero, G. Anciaux, A. Molinari, and J. F. Molinari, Friction at the toolchip interface during orthogonal nanometric machining, Model. Simul. Mater. Sci. Eng. **20**, 055007 (2012).
[7] P. A. Romero, G. Anciaux, A. Molinari, and J.-F. Molinari, Insights into the thermo-mechanics of orthogonal nanometric machining, Comput. Mater. Sci. **72**, 116 (2013).
[8] P. Berlet, M. Dienwiebel, and M. Scherge, The effect of sample finishing on the tribology of metal/metal lubricated contacts, Wear **268**, 1518 (2010).
[9] P. Iglesias, M. D. Bermúdez, W. Moscoso, and S. Chandrasekar, Influence of processing parameters on wear resistance of nanostructured ofhc copper manufactured by large strain extrusion machining, Wear **268**, 178 (2010).
[10] Peter J. Blau, On the nature of running-in, Tribol. Int. **38**, 1007 (2005).
[11] Narayan K. Sundaram, Yang Guo, and Srinivasan Chandrasekar, Mesoscale folding, instability, and disruption of laminar flow in metal surfaces, Phys. Rev. Lett. **109**, 106001 (2012).
[12] Philip G. Drazin and William Hill Reid, *Hydrodynamic stability* (Cambridge University Press, Cambridge, England, 2004).
[13] David A. Rigney and S. Karthikeyan, The evolution of tribomaterial during sliding: A brief introduction, Tribol. Lett. **39**, 3 (2010).
[14] Martin H. Müser and Sissi de Beer, Surface folds make tears and chips, Physics **5**, 100 (2012).
[15] A. Mahato, Y. Guo, N. Sundaram, T. G. Murthy, C. Saldana, and S. Chandrasekar, Unconstrained plastic flow at surfaces in sliding and cutting, Int. J. Precis. Technol. **3**, 370 (2013).
[16] K. J. Hemker and W. N. Sharpe, Jr., Microscale characterization of mechanical properties, Annu. Rev. Mater. Res. **37**, 93 (2007).
[17] Z. W. Shan, Raja K. Mishra, S. A. Syed Asif, Oden L. Warren, and Andrew M. Minor, Mechanical annealing and source-limited deformation in submicrometre-diameter Ni crystals, Nat. Mater. **7**, 115 (2008).
[18] Y. Liao, R. Pourzal, M. A. Wimmer, J. J. Jacobs, A. Fischer, and L. D. Marks, Graphitic tribological layers in metal-on-metal hip replacements, Science **334**, 1687 (2011).
[19] Xinyi Zhang, Reinhard Schneider, Erich Müller, Manuel Mee, Sven Meier, Peter Gumbsch, and Dagmar Gerthsen, Electron microscopic evidence for a tribologically induced phase transformation as the origin of wear in diamond, J. Appl. Phys. **115**, 063508 (2014).
[20] Steve Plimpton, Fast parallel algorithms for short-range molecular dynamics, J. Comput. Phys. **117**, 1 (1995).
[21] Y. Mishin, M. J. Mehl, D. A. Papaconstantopoulos, A. F. Voter, and J. D. Kress, Structural stability and lattice defects in copper: *Ab initio*, tight-binding, and embedded-atom calculations, Phys. Rev. B **63**, 224106 (2001).
[22] Erik Bitzek, Pekka Koskinen, Franz Gähler, Michael Moseler, and Peter Gumbsch, Structural relaxation made simple, Phys. Rev. Lett. **97**, 170201 (2006).
[23] Herman J. C. Berendsen, J. P. M. Postma, Wilfred F. van Gunsteren, A. R. H. J. DiNola, and J. R. Haak, Molecular

dynamics with coupling to an external bath, J. Chem. Phys. **81**, 3684 (1984).
[24] J. Dana Honeycutt and Hans C. Andersen, Molecular dynamics study of melting and freezing of small Lennard-Jones clusters, J. Phys. Chem. **91**, 4950 (1987).
[25] Pedro A. Romero, Tommi T. Järvi, Nils Beckmann, Matous Mrovec, and Michael Moseler, Coarse graining and localized plasticity between sliding nanocrystalline metals, Phys. Rev. Lett. **113**, 036101 (2014).
[26] Michael Chandross and Elizabeth A. Holm, Measuring grain junction angles in discretized microstructures, Metall. Mater. Trans. A **41**, 3018 (2010).
[27] D. P. Field, L. T. Bradford, M. M. Nowell, and T. M. Lillo, The role of annealing twins during recrystallization of Cu, Acta Mater. **55**, 4233 (2007).
[28] Diana Farkas, Eduardo Bringa, and Alfredo Caro, Annealing twins in nanocrystalline fcc metals: A molecular dynamics simulation, Phys. Rev. B **75**, 184111 (2007).
[29] Elizabeth A. Holm and Stephen M. Foiles, How grain growth stops: A mechanism for grain-growth stagnation in pure materials, Science **328**, 1138 (2010).
[30] Robert D. Groot and Patrick B. Warren, Dissipative particle dynamics: Bridging the gap between atomistic and mesoscopic simulation, J. Chem. Phys. **107**, 4423 (1997).
[31] A. Emge, S. Karthikeyan, and D. A. Rigney, The effects of sliding velocity and sliding time on nanocrystalline tribolayer development and properties in copper, Wear **267**, 562 (2009).
[32] See Supplemental Material at http://link.aps.org/supplemental/10.1103/PhysRevApplied.2.064004 for a detailed description of the atomistic model and the experiments as well as for movies showing the complete evolution of the fold and grain structure during the simulated plowing time.
[33] H. W. Sheng, M. J. Kramer, A. Cadien, T. Fujita, and M. W. Chen, Highly optimized embedded-atom-method potentials for fourteen fcc metals, Phys. Rev. B **83**, 134118 (2011).
[34] Y. Mishin, D. Farkas, M. J. Mehl, and D. A. Papaconstantopoulos, Interatomic potentials for monoatomic metals from experimental data and *ab initio* calculation, Phys. Rev. B **59**, 3393 (1999).
[35] P. L. Williams, Y. Mishin, and J. C. Hamilton, An embedded-atom potential for the CuAg system, Model. Simul. Mater. Sci. Eng. **14**, 817 (2006).
[36] Diana Farkas, Anders Frøseth, and Helena Van Swygenhoven, Grain boundary migration during room temperature deformation of nanocrystalline Ni, Scr. Mater. **55**, 695 (2006).
[37] L. Lu, X. Chen, X. Huang, and K. Lu, Revealing the maximum strength in nanotwinned copper, Science **323**, 607 (2009).
[38] Xiaoyan Li, Yujie Wei, Lei Lu, Ke Lu, and Huajian Gao, Dislocation nucleation governed softening and maximum strength in nano-twinned metals, Nature (London) **464**, 877 (2010).
[39] Jakob Schiotz and Karsten W. Jacobsen, A maximum in the strength of nanocrystalline copper, Science **301**, 1357 (2003).
[40] D. V. Bachurin and P. Gumbsch, Accommodation processes during deformation of nanocrystalline palladium, Acta Mater. **58**, 5491 (2010).
[41] David Dornfeld, Sangkee Min, and Y Takeuchi, Recent advances in mechanical micromachining, CIRP Ann. Manuf. Technol. **55**, 745 (2006).
[42] Yuanfeng Cheng, Daniel Weygand, and Peter Gumbsch, Simulation of small-angle tilt grain boundaries and their response to stress, Comput. Mater. Sci. **45**, 783 (2009).
[43] John W. Cahn, Yuri Mishin, and Akira Suzuki, Coupling grain boundary motion to shear deformation, Acta Mater. **54**, 4953 (2006).
[44] D. Helm, A. Butz, D. Raabe, and P. Gumbsch, Microstructure-based description of the deformation of metals: Theory and application, JOM **63**, 26 (2011).
[45] C. Y. Tang and W. H. Tai, Material damage and forming limits of textured sheet metals, J. Mater. Process. Technol. **99**, 135 (2000).
[46] S. W. Banovic, M. D. Vaudin, T. H. Gnaeupel-Herold, D. M. Saylor, and K.P Rodbell, Studies of deformation-induced texture development in sheet materials using diffraction techniques, Mater. Sci. Eng. A **380**, 155 (2004).
[47] D. Shakhvorostov, B. Gleising, R. Büscher, W. Dudzinski, A. Fischer, and M. Scherge, Microstructure of tribologically induced nanolayers produced at ultra-low wear rates, Wear **263**, 1259 (2007).
[48] Ruslan Valiev, Nanostructuring of metals by severe plastic deformation for advanced properties, Nat. Mater. **3**, 511 (2004).
[49] Y. Estrin and A. Vinogradov, Extreme grain refinement by severe plastic deformation: A wealth of challenging science, Acta Mater. **61**, 782 (2013).
[50] C. Saldana, S. Swaminathan, T. L. Brown, W. Moscoso, J. B. Mann, W. D. Compton, and S. Chandrasekar, Unusual applications of machining: Controlled nanostructuring of materials and surfaces, J. Manuf. Sci. Eng. **132**, 030908 (2010).
[51] N. Q. Vo, J. Schaefer, R. S. Averback, K. Albe, Y. Ashkenazy, and P. Bellon, Reaching theoretical strengths in nanocrystalline Cu by grain boundary doping, Scr. Mater. **65**, 660 (2011).
[52] Sezer Ouzerin, Kaiping Tai, Nhon Q. Vo, Pascal Bellon, Robert S. Averback, and William P. King, Grain boundary doping strengthens nanocrystalline copper alloys, Scr. Mater. **67**, 720 (2012).
[53] Ajay P Malshe, Wenping Jiang, and Ajit R Dhamdhere, Nanostructured coatings for machining and wear-resistant applications, JOM **54**, 28 (2002).
[54] Alexander Stukowski, Visualization and analysis of atomistic simulation data with OVITO—the Open Visualization Tool, Model. Simul. Mater. Sci. Eng. **18**, 015012 (2010).
[55] Alexander Stukowski, Automated identification and indexing of dislocations in crystal interfaces, Model. Simul. Mater. Sci. Eng. **20**, 085007 (2012).